

Temporally Correlated Narrowband Biphoton Interference Based on Mach–Zehnder Interferometer

Da Zhang, Irfan Ahmed, Lin Hao, Yin Cai, Changbiao Li, Yiqi Zhang, and Yanpeng Zhang*

Since early 1990s, Mach–Zehnder interferometer has been used to investigate the interference of biphoton wave packets. Due to subpicosecond time coherence of biphoton generated by spontaneous parametric downconversion process, some physical processes are ignored in the interferometer, most likely the biphoton time-domain interference. Here, the two-photon interference phenomenon based on the Mach–Zehnder interferometer is theoretically studied, where the correlated photon pairs are produced by the four-wave mixing in atomic system. In particular, the quantum interference effect to effectively control the coherent time of two-photon by adjusting the input delay is used. In the damped Rabi oscillation regime, two-photon bunching and antibunching effects are observed. In addition, in the group-delay regime, the interference between biphoton precursor, slow-light wave packets and also in between the precursor and the slow-light wave packets is observed, which had never been reported before. These results may have potential applications in the fields of biphoton shaping and quantum information processing.

has been understood as a phenomenon that occurs when two indistinguishable wave packets are input to two input channels of the beam splitter (BS). So far, the observation of two-photon interference effects have been regarded as a basic step toward the photonic quantum information technology because of its diverse applications in quantum information, such as quantum key distribution,^[4,5] quantum repeaters,^[6] and quantum computing.^[7–9] Among those, the degree of freedom (DoF) of HOM interference mainly includes path,^[3,10] polarization,^[11] energy–time,^[12] and frequency.^[13] On the other hand, the physical system observing the interference effect of HOM has also rapidly expanded from spontaneous parametric downconversion (SPDC) to quantum dots,^[14] trapped ions,^[15] nitrogen-vacancy centers,^[16] silicon-vacancy centers,^[17] and surface plasmons.^[18]

1. Introduction

Quantum interference and entanglement using a pair of correlated photons have played an important role in fundamental investigations of quantum mechanics^[1] and the exploration of quantum information technology.^[2] Since, the observation of Hong–Ou–Mandel (HOM) interference experiment in 1987,^[3] it


The core of two-photon quantum interference is the indistinguishable two-photon probability amplitudes in quantum measurement. In other words, the interference can be observed even if the photons are distinguishable when they arrive the BS. The key idea is to hide distinguishable information before measurement.^[19,20] For example, in the HOM experiment, if photons in one input channel reaches the BS earlier than the photon in the other channel, then we can distinguish the r–r and t–t paths by the timing information, and there is no interference. If an extra path is introduced to hide the trigger information, we can restore the interference again by choosing the appropriate delay.^[19] The same principles can be applied to the interference experiments of polarization.^[11] The overlap of two-photon wave packets is no longer a necessary condition for two-photon interference. Thus, some interesting phenomena appeared, such as quantum interference and entanglement of photons that do not overlap in time,^[21] the entanglement exchange between two photon pairs that do not coexist.^[22]

As early as 30 years ago, the Mach–Zehnder interferometer (MZI) has been utilized to investigate two-photon wave packet interference phenomena.^[23,24] No input delay remains one of the most common means of doing so,^[10,25] which plays an important role in quantum metrology. In principle, using quantum resources, the uncertainty in measuring an optical phase φ with an interferometer is likely to dramatically improve

Dr. D. Zhang, L. Hao, Prof. Y. Cai, Prof. C. Li, Prof. Y. Zhang, Prof. Y. Zhang
Key Laboratory for Physical Electronics and Devices of the Ministry of Education & Shaanxi Key Lab of Information Photonic Technique
Xi'an Jiaotong University
Xi'an 710049, China
E-mail: ypzhang@mail.xjtu.edu.cn

Dr. I. Ahmed
Department of Physics
City University of Hong Kong
Kowloon 999077, Hong Kong Special Administrative Region
China

Dr. I. Ahmed
Electrical Engineering Department
Sukkur IBA University
Sindh 65200, Pakistan

 The ORCID identification number(s) for the author(s) of this article can be found under <https://doi.org/10.1002/andp.201900300>

DOI: 10.1002/andp.201900300

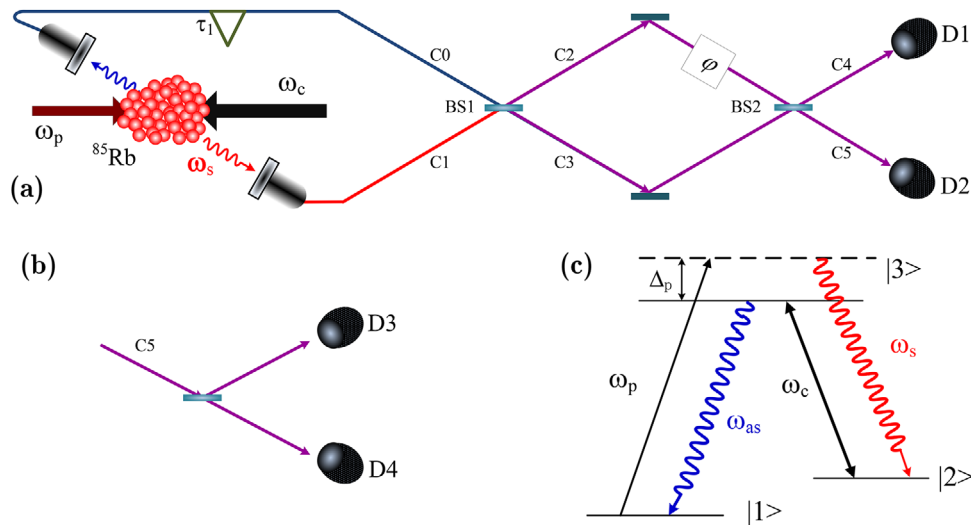


Figure 1. The schematic diagram of two-photon interference. a) MZI. BS, beam splitter; D, single-photon detector. b) Two-photon coincidence counting demonstration in C_5 channel. c) The energy level diagram of FWM process.

on the standard quantum limit and reach up the Heisenberg limit.^[26–28]

In most quantum optics experiments, the temporal coherence of the biphoton source generated by SPDC is on the order of subpicosecond, which is much shorter than the response time of the current photodetectors. Therefore, the biphoton interference in time-domain is neglected. Instead of SPDC, the photon pairs produced by four-wave mixing (FWM) in atomic medium have long temporal correlated nature.^[29–33] Similarly, the HOM effect has been experimentally observed between the narrowband biphoton.^[12] Furthermore, based on the double- Λ atomic configuration, many interesting schemes have been experimentally implemented, such as frequency-induced phase-tunable polarization-entangled biphoton,^[34] hyper-entanglement,^[35,36] testing the Bell inequality on frequency-bin entangled photon pairs^[37]. However, narrowband biphoton interference based on MZI has not been reported, especially in group-delay regime.^[38,39] Therefore, in this paper, we shall comprehensively study the quantum interference of narrowband biphoton based on the MZI, including the damped Rabi oscillation wave packets and the group-delay wave packets.

The paper is organized as follows. In Section 2, we review the general formalism of the biphoton wave packet generated from the FWM in the Heisenberg picture. We study the biphoton wave packet interference in a conventional MZI in Section 3 employing damped Rabi oscillation and group-delay regimes. In the damped Rabi oscillation regime, the two-photon wave packet interference exhibits completely different physical properties, such as time-domain and path wave packets, are interdependent or independent of each other under different quantum measurement protocols. Two-photon bunching and antibunching effects are observed by adjusting the input delay. In the group-delay regime, we observed the interference between biphoton precursor, slow-light wave packets and between the precursor and the slow-light wave packets, which had never been reported before. Finally, we draw the conclusion and outlook in Section 4.

2. Spontaneous Parametric Four-Wave Mixing

In Figure 1a, we present the schematic to study two-photon interference effect. It contains two parts: two-photon source, which produces correlated photon pairs via FWM, and the MZI. The measurement protocol also includes two types, R_{45} as shown in Figure 1a and R_{55} as shown in Figure 1b, respectively. We first consider the generation of the narrowband biphoton in a double- Λ cold atomic system with length L (see Figure 1c). The cold atoms are identical and prepared in ground state $|1\rangle$. A weak pump laser with angular frequency ω_p (Rabi frequency Ω_p) and a strong coupling field with angular frequency ω_c (Rabi frequency Ω_c) are set to counter-propagate through the medium. The weak pump beam is applied to the atomic transition $|1\rangle \rightarrow |3\rangle$ with a detuning $\Delta_p = \omega_{31} - \omega_p$, and a strong coupling laser is resonant on the transition $|2\rangle \rightarrow |3\rangle$. ω_{ij} is the transition frequency between levels $|i\rangle$ and $|j\rangle$. Paired Stokes and anti-Stokes photons are spontaneously produced from the FWM process in the low-gain limit. Here, we shall follow the degenerated photon pairs with pump detuning $\Delta_p = \Delta_{21}$, where Δ_{21} is the hyperfine splitting between $|1\rangle$ and $|2\rangle$. Thus, the central-frequency difference between the Stokes and anti-Stokes photons is zero. The phase-matching condition allows the generation of backward propagating paired photons in a right-angle geometry.

The single-transverse-mode anti-Stokes and Stokes fields are taken as quantized

$$E_{as}^{(+)}(z, t) = \frac{E_{as}}{\sqrt{2\pi}} \int d\omega_{as} \hat{a}_{as}(z, \omega_{as}) e^{i(-k_{as}z - \omega_{as}t)}$$

$$E_s^{(+)}(z, t) = \frac{E_s}{\sqrt{2\pi}} \int d\omega_s \hat{a}_s(z, \omega_s) e^{i(k_s z - \omega_s t)} \quad (1)$$

Here $E_{a/as} = \sqrt{2\hbar\omega_{s/as}/c\epsilon_0 A}$, ω_{as} (ω_s) is the central frequency of the anti-Stokes (Stokes) photon, c is the speed of light in vacuum, ϵ_0 is the vacuum permittivity, and A is the single-mode

cross-sectional area. k_j ($j = s, as$) are wave numbers and \hat{a}_j are the annihilation operators at the output surface associated with k_j .

Assuming that the coupling and pump fields are undepleted in the FWM process and working in the Heisenberg picture, the operator $\hat{a}_j(z, \omega_j)$ is governed by the coupled propagation equations under the slowly varying envelope approximation

$$\begin{aligned} \frac{d\hat{a}_s^+(z, \omega_s)}{dz} &= \kappa_s \hat{a}_{as}(z, \omega_{as}) - \left(g_s + i \frac{\delta k_0}{2} \right) \hat{a}_s^+(z, \omega_s) \\ \frac{d\hat{a}_{as}(z, \omega_{as})}{dz} &= \kappa_{as} \hat{a}_s^+(z, \omega_s) - \left(g_{as} - i \frac{\delta k_0}{2} \right) \hat{a}_{as}(z, \omega_{as}) \end{aligned} \quad (2)$$

In Equation (2), κ_s and κ_{as} are the parametric coupling coefficients and are determined by the third-order susceptibilities $\chi^{(3)}$, where $\kappa_s = i\chi_s^{(3)} E_p^* E_c^* / 2c$ and $\kappa_{as} = i\chi_{as}^{(3)} E_p E_c / 2c$, while g_s and g_{as} are (complex) gains for Stokes and anti-Stokes beams, respectively. These complex gains are determined from the linear susceptibilities χ_j , where $g_s = i\varpi_s \chi_s^* / 2c$ and $g_{as} = i\varpi_{as} \chi_{as} / 2c$. $\delta k_0 = k_p - k_c + k_{as} - k_s$ is the phase-mismatching term in vacuum. Since the pump is far from resonance and much weaker than the coupling field, the quantum atomic noise may likely be suppressed while the atomic population can be maintained primarily in the ground state. Thus, the influence of quantum Langevin noise fluctuation in coincidence counting regime is neglected.^[29,40–42] In the two-photon level, the quantum Langevin noise introduces unpaired photons, which are not of interest here. On the other hand, the validity of neglecting Langevin noises in the two-photon correlation in a cascade amplifier has been discussed in ref. [43]. The nonlinear and linear susceptibilities are given in ref. [44]. It is to be noted that κ_s , g_s , κ_{as} , g_{as} , and δk_0 are functions of ω .

The solution of Equation (2) may be written as a linear combination of the following boundary conditions

$$\begin{aligned} [\hat{a}_s(0, \omega), \hat{a}_s^+(0, \omega')] &= [\hat{a}_{as}(L, \omega), \hat{a}_{as}^+(L, \omega')] = \delta(\omega - \omega') \\ \langle \hat{a}_s(0, \omega) \hat{a}_s^+(0, \omega) \rangle &= \langle \hat{a}_{as}(L, \omega) \hat{a}_{as}^+(L, \omega) \rangle = 1 \end{aligned} \quad (3)$$

Briefly, the photons pairs are initially generated from the quantum fluctuations and vacuum. The solution of Equation (2) at the output surface has the following form

$$\begin{aligned} \hat{a}_s^+(L, \omega) &= Q_{s1} \hat{a}_s^+(0, \omega) + Q_{as1} \hat{a}_{as}(L, \omega) \\ \hat{a}_{as}(0, \omega) &= Q_{s2} \hat{a}_s^+(0, \omega) + Q_{as2} \hat{a}_{as}(L, \omega) \end{aligned} \quad (4)$$

where

$$\begin{aligned} Q_{s1} &= \frac{-\frac{q_3}{\kappa_{as}} e^{\lambda_1 L + \lambda_2 L}}{\left(\frac{q_2 - q_3}{2\kappa_s} e^{\lambda_1 L} - \frac{q_2 + q_3}{2\kappa_{as}} e^{\lambda_2 L} \right)} \\ Q_{as1} &= \frac{(e^{\lambda_2 L} - e^{\lambda_1 L})}{\left(\frac{q_2 - q_3}{2\kappa_s} e^{\lambda_1 L} - \frac{q_2 + q_3}{2\kappa_{as}} e^{\lambda_2 L} \right)} \\ Q_{s2} &= \frac{(e^{\lambda_2 L} - e^{\lambda_1 L})}{\left(\frac{q_2 - q_3}{2\kappa_s} e^{\lambda_1 L} - \frac{q_2 + q_3}{2\kappa_{as}} e^{\lambda_2 L} \right)} \end{aligned}$$

$$Q_{as2} = \frac{-\frac{q_3}{2\kappa_{as}}}{\left(\frac{q_2 - q_3}{\kappa_s} e^{\lambda_1 L} - \frac{q_2 + q_3}{2\kappa_{as}} e^{\lambda_2 L} \right)}$$

Here, $\lambda_1 = (-q_0 - q_3)/2$, $\lambda_2 = (-q_0 + q_3)/2$, $q_0 = g_s + g_{as}$, $q_2 = g_{as} - g_s + i\delta k_0$, and $q_3 = \sqrt{q_2^2 + 4\kappa_{as}\kappa_s}$. In the limit of low parametric gain,^[45,46] that is, $q_3 \approx q_2$, Equation (4) reduces to

$$\begin{aligned} \hat{a}_{as}(0, \omega) &= -\frac{\kappa_{as}(1 - e^{-q_2 L})}{q_2} \hat{a}_s^+(0, \omega) + e^{-\lambda_2 L} \hat{a}_{as}(L, \omega) \\ \hat{a}_s^+(L, \omega) &= e^{\lambda_1 L} \hat{a}_s^+(0, \omega) - \frac{\kappa_{as}(1 - e^{-q_2 L})}{q_2} \hat{a}_{as}(L, \omega) \end{aligned} \quad (5)$$

The second-order intensity correlation function can be written as

$$G^{(2)} = \langle E_s^{(-)} E_{as}^{(-)} E_{as}^{(+)} E_s^{(+)} \rangle = |B(\tau_s, \tau_{as})|^2 + R_s R_{as} \quad (6)$$

where $\tau_j = t_j - r_j/c$, r_j is the optical path from the output surface of the medium to the detector, t_j is the trigger time. For simplicity, we choose $r_s = r_{as}$. In general, the function $B(\tau_s, \tau_{as})$ is referred as the two-photon amplitude, or biphoton wave packet. It has the form

$$B(\tau) = B_1 e^{i(\omega_c + \omega_p)\tau_{as}} \int d\omega e^{-\lambda_2 L} \frac{\kappa_{as}(1 - e^{-q_2 L})}{q_2} e^{-i\omega\tau} \quad (7)$$

where $\tau = t_s - t_{as}$ and $B_1 = -\hbar \sqrt{\varpi_s \varpi_{as}} / (\pi c \epsilon_0 A)$. In the medium, the Stokes wave number is $k_{s1} \approx \varpi_s / c(1 + \chi_s/2) = k_s + \Delta k_s$, and the anti-Stokes wave number is $k_{as1} \approx \varpi_{as} / c(1 + \chi_{as}/2) = k_{as} + \Delta k_{as}$. For the Stokes field, the Raman gain is small because of $\chi_s \approx 0$, Δk_s^* can be approximated as Δk_s . Then $q_2 = i\Delta k_{as} - i\Delta k_s^* + i\delta k_0 = i\delta k$, $\lambda_1 = i(\Delta k_s + \Delta k_{as})/2 - i\delta k/2$, and $\lambda_2 = i(\Delta k_s + \Delta k_{as})/2 + i\delta k/2$. δk is the phase mismatching in the medium. Based on above analysis, Equation (7) becomes

$$\begin{aligned} B(\tau) &= B_1 L e^{-i(k_s + k_{as})L/2} e^{i(\omega_c + \omega_p)\tau_{as}} \int d\omega e^{-i\omega\tau} \kappa_{as} \\ &\quad \times \Phi(\delta k L) \end{aligned} \quad (8)$$

where $\Phi(\delta k L) = \text{sinc}(\delta k L/2) e^{i(k_{s1} + k_{as1})L/2}$ is the longitudinal detuning function, which carries the phase mismatch information in the longitudinal direction over the entire medium.

Working in the damped Rabi oscillation regime,^[29,44,47] the biphoton wavepackets are mainly determined by the third-order nonlinear susceptibility. In such a case, the longitudinal detuning function Φ is approximated to 1. The two-photon amplitude has the form

$$B(\tau_s) = B_2 e^{i(\omega_p + \omega_c)\tau_{as}} \sin(\Omega_c \tau/2) e^{-\gamma_e \tau} \Theta(\tau) \quad (9)$$

B_2 has absorbed all constants and slowly varying terms. γ_e represents the effective dephasing rate.^[44] The heaviside step function is defined here as $\Theta(\tau) = 1$ for $\tau \geq 0$, and $\Theta(\tau) = 0$ for $\tau < 0$. In Equation (5), the term $R_s R_{as}$ results from accidental coincidence between uncorrelated photons as the photon pairs are stochastically produced in time and space. They have the form

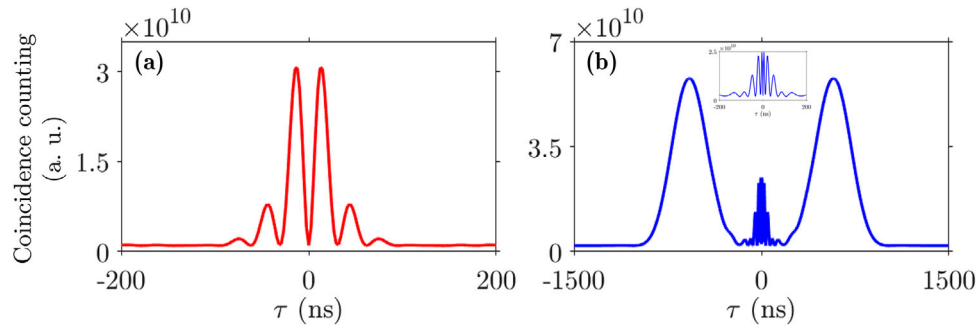


Figure 2. The two-photon coincidence counting in the a) damped Rabi oscillation regime and b) group-delay regime.

$R_{s/as} = \hbar \varpi_{s/as} / (\pi \epsilon_0 c A) \int d\omega (\kappa_{s/as} \Phi e^{-i\omega\tau})^2$. Considering the generation of backward propagating paired photons in a right-angle geometry, the coincidence counting has the form

$$R_{cc} = W_1 [1 - \cos(\Omega_c |\tau|)] e^{-2\gamma_c |\tau|} + R_s R_{as} \quad (10)$$

where W_1 is a constant. **Figure 2a** is the numerical simulation of two-photon coincidence counting in the damped Rabi oscillation regime. The parameters we selected are $L = 2.5\text{cm}$, $\gamma_e = 2\pi \times 1.53\text{MHz}$, $\Omega_p = 2\pi \times 1.97\text{MHz}$, $\Omega_c = 2\pi \times 33.3\text{MHz}$, and $OD = 10$. The two-photon correlation exhibits damped Rabi oscillations of period $2\pi/\Omega_c$. The observed antibunching-like effect at $\tau = 0$ is due to the destructive interference between two types of biphoton generation.^[29,44,46,47]

In the group-delay regime, nonlinear response of biphoton is washed out due to the electromagnetically induced transparency slow light. Since Stokes and anti-Stokes photons have the same center frequency, they both experience slow light effects. The resulting wave-number mismatch is modified as $\delta k = 2\omega/v_{as}$ (v_{as} is group velocity of anti-Stokes photons through the system) and the nonlinearity response is regarded as constant. **Figure 2b** is a numerical simulation of two-photon coincidence counting in the group-delay regime. The parameters are the same as in **Figure 2a** except $\Omega_c = 2\pi \times 8.15\text{MHz}$ and $OD = 150$. Near the zero point, the waveform behaves like wheat spike is a two-photon precursor, which is produced by atomic radiation at the center of system. Illustrated as an enlarged image of two-photon precursor, its physical properties depend on the Rabi frequency of coupling field and the OD of the atomic medium. We can see that the precursor and the slow-light wave packet have been separated, and the coherence time reaches 1000 ns.

3. Two Photons Interference Based on MZI

In this section, the two-photon interference phenomenon is investigated based on MZI, which is composed of two lossless BSs as shown in **Figure 1a**. In particular, we introduce a delay $\tau_1 = \Delta L_1/c$ in C_0 channel, where ΔL_1 is optical path-length difference between the two photons at the BS1 input stage. If we set $\tau_1 = 0$, the classical biphoton $N00N$ states are generated via the HOM interference effect at either arm of the interferometer (C_2 or C_3).^[3] Interestingly, the produced $N00N$ state are entangled not only in path, but also in energy–time, which can be measured in experiments. Then, the two paths are combined at BS2, and the

biphoton interference is measured by two different methods. One is measured at the two output ports C_4 and C_5 by the D_1 and D_2 detectors. The other is measured at the output port C_5 of BS2 as shown in **Figure 1b**. The input–output operators are connected by the scattering matrices of the BS and the optical path-length difference and their Hermitian conjugates $A_{out} = U_{BS} U_{path} U_{BS} A_{in}$, where $A_{out} = (a_4, a_5)^T$, $A_{in} = (a_0, a_1)^T$ and

$$U_{BS} = \frac{1}{\sqrt{2}} \begin{pmatrix} 1 & i \\ i & 1 \end{pmatrix}, \quad U_{path} = \begin{pmatrix} 1 & 0 \\ 0 & e^{i\varphi} \end{pmatrix} \quad (11)$$

In Equation (11), φ is the optical phase difference between the C_2 and C_3 channels. The input operator A_{in} has the form $\hat{a}_0 = e^{-i\omega_{as}/s\tau_1} [\hat{a}_{as}(0, \omega) + \hat{a}_s(0, \omega)]$ and $\hat{a}_1 = \hat{a}_s(L, \omega) + \hat{a}_{as}(L, \omega)$.

After complex calculation, one obtains the two-photon wave packets at the output channels as

$$B_{45} = \frac{1}{4} [B(|\tau - \tau_1|) \otimes (1 - 2e^{i\varphi} + e^{i2\varphi}) + B(|\tau + \tau_1|) \otimes (1 + 2e^{i\varphi} + e^{i2\varphi})] \quad (12)$$

$$B_{55} = \frac{1}{4} [B(|\tau - \tau_1|) + B(|\tau + \tau_1|)] \otimes (1 - e^{i2\varphi}) \quad (13)$$

Obviously, the two-photon amplitudes B_{45} and B_{55} are composed of two DoFs, energy–time and path (represented by phase information), which are related to each other in B_{45} and independent of each other in B_{55} . Now the physics is clear. Following BS1, the time-domain wave packets $B(|\tau - \tau_1|)$ and $B(|\tau + \tau_1|)$ are generated. In B_{45} , the $B(|\tau - \tau_1|)$ and $B(|\tau + \tau_1|)$ have different phases inside the MZI, while they are same in B_{55} . This can be seen through the energy–time DoF that B_{55} embodies the quantum properties of the light field while B_{45} does not. On the other hand, focusing on the time-domain correlation, we find that the biphoton amplitude through MZI, is transformed as the coherent superposition of $B(|\tau - \tau_1|)$ and $B(|\tau + \tau_1|)$ whether in B_{45} or B_{55} . In comparison with the two-photon amplitude $[B(\tau - \tau_1) + B(-\tau + \tau_1)]$ prior to input, the biphoton coherence time is extended by τ_1 after the MZI. That is, using the quantum interference effect the coherence time of biphoton can be extended by adjusting the import delay. Of course, the price is consistent with a reduction in the coincidence counting.

If we assume $\tau_1 = 0$, the path information carried by the two-photon wave amplitude in B_{45} degenerates to $(1 + e^{i2\varphi})$, which is consistent with previously reported results.^[10,48]

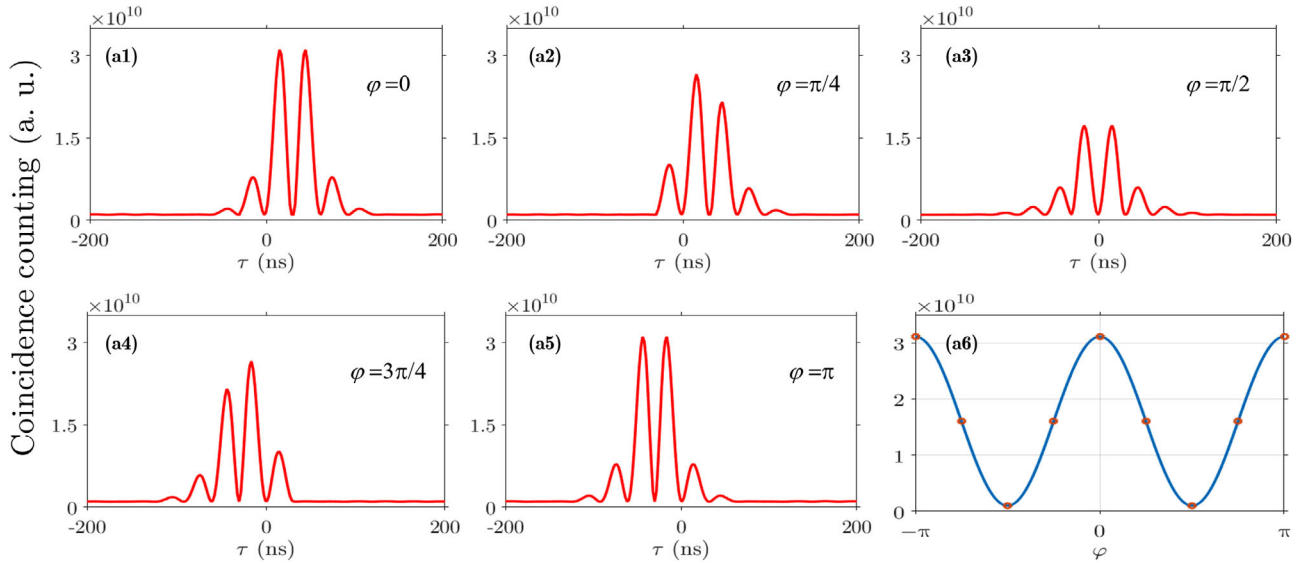


Figure 3. Interference fringes obtained for two-photon coincidence counting R_{45} with fixed delay.

Assuming perfect detection efficiency, the two-photon coincidence counting is given as

$$R_{45} = \frac{1}{16} [B^2(|\tau + \tau_1|) + R_{as}R_s](6 + 2\cos 2\varphi - 8\cos \varphi) + B^2(|\tau - \tau_1|) + R_{as}R_s(6 + 2\cos 2\varphi + 8\cos \varphi) + 4[B(|\tau + \tau_1|)B(|\tau - \tau_1|) + R_{as}R_s](1 - \cos 2\varphi)] \quad (14)$$

$$R_{55} = \frac{1}{8} [B^2(|\tau + \tau_1|) + B^2(|\tau - \tau_1|) + 4R_{as}R_s + 2B(|\tau + \tau_1|)B(|\tau - \tau_1|)](1 - \cos 2\varphi) \quad (15)$$

There is no temporal interference between the uncorrelated photon pairs. Considering the related phase information of $B(|\tau - \tau_1|)$ and $B(|\tau + \tau_1|)$, the MZI provides a precise control for two-photon wave packet shaping. It is worth mentioning that the shaping effects of R_{45} and R_{55} are not the same. If we set $\tau_1 = 0$ and $\varphi = 0$, Equation (14) will degenerate to Equation (10). When $\tau_1 = 0$ and $\varphi = \pi/2$, Equation (15) degenerates to Equation (10).

Figure 3 shows the numerical simulation of the coincidence counts R_{45} , in which the biphoton wave packets are determined by the nonlinear response. The parameters are the same as in Figure 2a. In Figure 3a1–a5, with a fixed delay $\tau_1 = 30$ ns, the biphoton time-domain wave packet changes from the right to the left as the phase φ varies from 0 to π . This is caused by the superposition of different energy–time and path wave packets. When $\varphi = 0$, path wave packet (phase) of $B(|\tau + \tau_1|)$ and $B(|\tau - \tau_1|)$ are going to be constructive and destructive interference, respectively. The situation is reversed with $\varphi = \pi$. In the intermediate transition region ($0 < \varphi < \pi$), biphoton wave packets $B(|\tau + \tau_1|)$ and $B(|\tau - \tau_1|)$ will interfere with each other. When $\varphi = \pi/2$, we can extract the phase information and then the time-domain wave packet will interfere with equal amplitudes. The path interference under a fixed input delay τ_1 is shown in Figure 3a6,

the coincidence counting oscillates with phase difference in the form of $(1 + \cos 2\varphi)$. Although, the oscillation period is the same as that of R_{55} , its physical essence is totally different, which has been reported in many literature. On the other hand, the path interference is not the subject of this paper, so it will not be emphasized here.

Next, we fixed φ to study the interference of the two-photon wave packets in time domain. As shown in **Figure 4**, by adjusting the delay τ_1 of C_0 arm, we can observe abundant interference phenomena. The initial delay is 150 ns, which is much larger than the two-photon coherence time (90 ns). We have not observed interference. As we reduce the delay to 90 ns, some slight interference phenomena appeared. With the further reduction of τ_1 , the overlap of $B(|\tau + \tau_1|)$ and $B(|\tau - \tau_1|)$ is getting larger and larger, and the interference phenomenon became more obvious. When $\tau_1 = 0$, $B(|\tau + \tau_1|)$ and $B(|\tau - \tau_1|)$ are completely coincident, and the time-domain wave packet is the same as that of Figure 2a, which is easy to comprehend. It is worth mentioning that $B(|\tau + \tau_1|)$ and $B(|\tau - \tau_1|)$ are producing constructive interference in the whole process. On the other hand, the coherence time of biphoton increases by τ_1 after the interference compared to the initial coherence time of 90 ns, which is of course at the expense of reducing the coincidence counting. The other feature is that the coincidence count R_{55} exhibits the photon antibunching effect at $\tau = 0$ in Figure 4a2,a5,a9, and the photon bunching effect is exhibited in other figures. The essential reason is that in the damped Rabi oscillation regime, the oscillation period is 30 ns. In case of $\tau_1 = n \times 30$ ns, ($n \in \mathbb{R}$), the two-photon amplitude reaches its minimum at $\tau = 0$, and their superposition is still the smallest, so the antibunching effect is exhibited. In other delay regions, the value of $B(|\tau + \tau_1|)$ and $B(|\tau - \tau_1|)$ at $\tau = 0$ are in the middle. Especially at $\tau_1 = 15$ ns, the two-photon time-domain wave packet takes the maximum value at $\tau = 0$.

In **Figure 5**, we study the interference of two-photon wave packet in the group-delay regime. The parameter settings are the same as those in Figure 2b. Due to large optical depth, the biphoton precursor and slow-light bodies have been separated, which

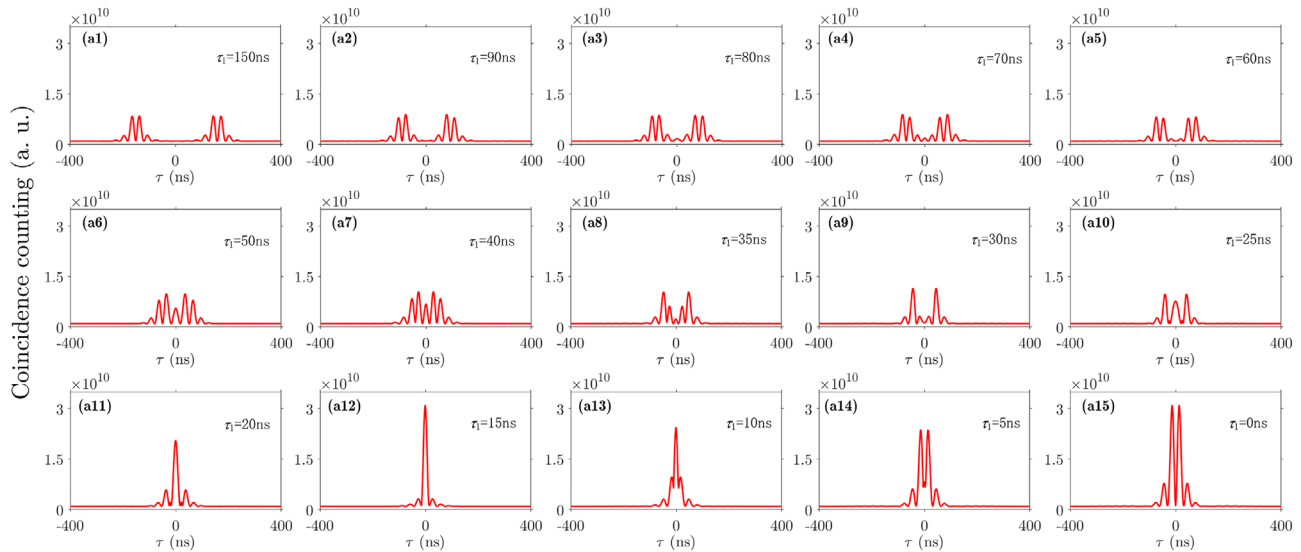


Figure 4. Interference fringes obtained for two-photon coincidence counting R_{55} with fixed phase difference φ .

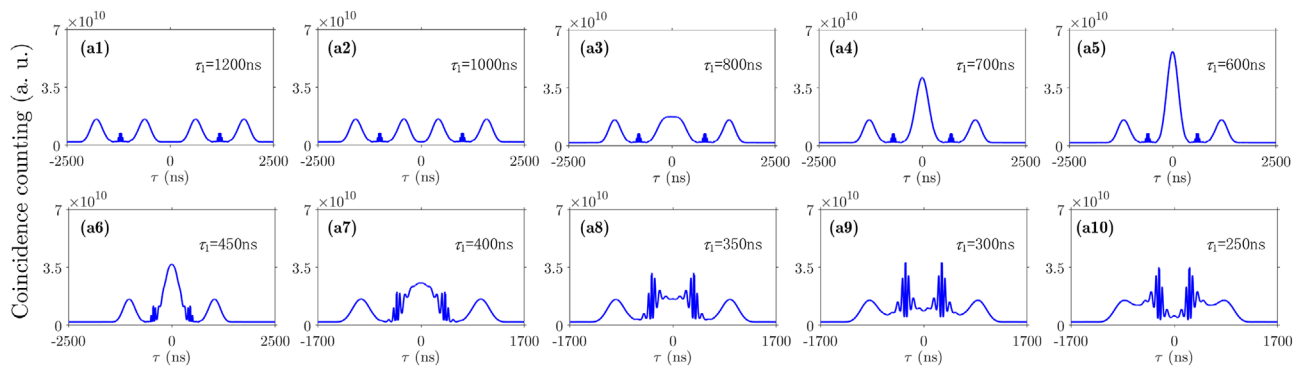


Figure 5. Same as Figure 4 but in group-delay regime.

provides richer interference pattern. Similarly, by adjusting the φ , coincidence counting R_{45} exhibits the same variation pattern as in the damped Rabi oscillation regime with the fixed delay, except for the biphoton shape. As shown in Figure 5a, no interference is observed for τ_1 greater than the coherence time of the two photon. When τ_1 is reduced to 1000 ns, the slow-light wave packets of $B(|\tau + \tau_1|)$ and $B(|\tau - \tau_1|)$ are at the critical point of interference. In other word, the coherent time of biphoton has extended to 2000 ns. With further reduction of τ_1 , the constructive interference of slow-light wave packet starts to occur (Figure 5a2–a6), and reaches its maximum value at $\tau_1 = 600$ ns. Continuing to reduce τ_1 (from 600 to 200 ns), the two-photon precursor of $B(|\tau - \tau_1|)$ and the slow-light wave packet of $B(|\tau + \tau_1|)$ appear with interference phenomenon on the right side of $\tau = 0$ (Figure 5a6–a10), and the opposite on the left. The magnitude is increasing gradually and interference pattern in the middle transits from the bulge to the dent. We have found that the interference fringes are smooth in the case of slow-light wave packet interference. When the two-photon precursor and slow-light wave packets interfere with each other, the interference pattern exhibits oscillation similar to that of the precursor, which suggests that the nature of the interference mainly depends on the property of the

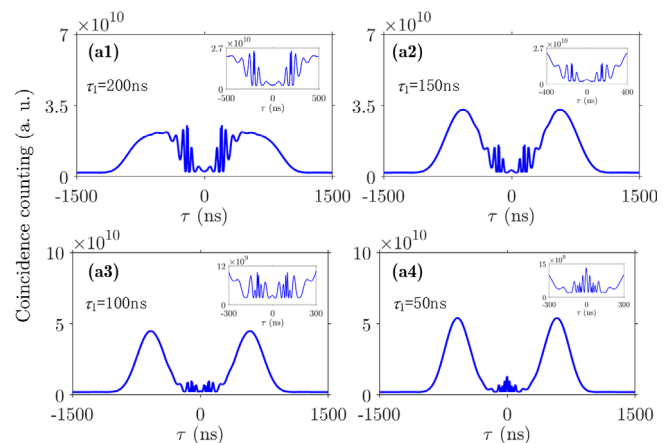


Figure 6. Same as Figure 5 but τ_1 is less than or equal to 200 ns.

two-photon precursor. In addition, there is interference between slow-light wave packets in this interval.

If τ_1 is less than or equal to 200 ns, as shown in Figure 6a1–a4, the two-photon precursor begins to interfere, and the inset is

an enlarged view of the precursor wave interference. Of course, there are interferences between the slow-light wave packets, and between the slow-light wave packets and the precursor. It is important to note that, as the input delay decreases (from 200 to 50 ns), so is the two-photon coherent time. In other words, we can adjust the coherence time of the biphoton at the output port of the interferometer by adjusting the input delay τ_1 . As τ_1 decreases, the amplitude of the slow-light wave packets gradually increases. When $\tau_1 = 0$ ns, $B(|\tau + \tau_1|)$ and $B(|\tau - \tau_1|)$ are completely coincident, and the result is the same as that in Figure 2b.

4. Conclusion

In summary, we studied the narrow-band two-photon time-domain interference phenomenon based on MZI, assisted by the long coherence time of two photon generated by FWM. By adjusting the input delays, we observed rich two-photon interference phenomenon, whether in the damped Rabi oscillation regime or the group-delay regime, which has not been reported before, especially the interference between slow-light wave packets, two-photon precursor, and interference between precursor and slow-light wave packets. Besides, the biphoton coherent time can be effectively regulated by import delay.

Our scheme is easy to implement in experiment. At the current experimental level, there is no problem to prepare cold atomic systems with large optical depth, for example, 150. Regarding the MZI, it is more convenient to use the optical fiber MZI despite the existence of certain loss. In addition, the input delay before BS1 can be regulate by adjusting the length of the fiber. It is hoped that our results can be applied to two-photon wave packet shaping and quantum information processing.

Acknowledgements

This work was supported by the National Key R&D Program of China (2017YFA0303703), National Natural Science Foundation of China (61605154, 11604256, and 11804267), and the Fundamental Research Funds for the Central Universities (Grant No. XJ2018206).

Conflict of Interest

The authors declare no conflict of interest.

Keywords

four-wave mixing, quantum metrology, two-photon interference

Received: July 7, 2019

Revised: September 16, 2019

Published online: October 14, 2019

- [1] A. Einstein, B. Podolsky, N. Rosen, *Phys. Rev.* **1935**, 47, 777.
 [2] V. Giovannetti, S. Lloyd, L. Maccone, *Phys. Rev. Lett.* **2006**, 96, 010401.
 [3] C. K. Hong, Z. Y. Ou, L. Mandel, *Phys. Rev. Lett.* **1987**, 59, 2044.

- [4] Y. L. Tang, H. L. Yin, S. J. Chen, Y. Liu, W. J. Zhang, X. Jiang, L. Zhang, J. Wang, L. X. You, J. Y. Guan, D. X. Yang, Z. Wang, H. Liang, Z. Zhang, N. Zhou, X. Ma, T. Y. Chen, Q. Zhang, J. W. Pan, *Phys. Rev. Lett.* **2014**, 113, 190501.
 [5] J. Y. Guan, Z. Cao, Y. Liu, G. L. Shen-Tu, J. S. Pelc, M. M. Fejer, C. Z. Peng, X. Ma, Q. Zhang, J. W. Pan, *Phys. Rev. Lett.* **2015**, 114, 180502.
 [6] N. Sangouard, C. Simon, H. de Riedmatten, N. Gisin, *Rev. Mod. Phys.* **2011**, 83, 33.
 [7] P. Kok, W. J. Munro, K. Nemoto, T. C. Ralph, J. P. Dowling, G. J. Milburn, *Rev. Mod. Phys.* **2007**, 79, 135.
 [8] J. Chen, K. F. Lee, P. Kumar, *Phys. Rev. A* **2007**, 76, 031804.
 [9] J. He, B. A. Bell, A. Casas-Bedoya, Y. Zhang, A. S. Clark, C. Xiong, B. J. Eggleton, *Optica* **2015**, 2, 779.
 [10] K. Edamatsu, R. Shimizu, T. Itoh, *Phys. Rev. Lett.* **2002**, 89, 213601.
 [11] Y. H. Shih, C. O. Alley, *Phys. Rev. Lett.* **1988**, 61, 2921.
 [12] C. Liu, J. F. Chen, S. Zhang, S. Zhou, Y. H. Kim, M. M. T. Loy, G. K. L. Wong, S. Du, *Phys. Rev. A* **2012**, 85, 021803.
 [13] T. Kobayashi, R. Ikuta, S. Yasui, S. Miki, T. Yamashita, H. Terai, T. Yamamoto, M. Koashi, N. Imoto, *Nat. Photonics* **2016**, 10, 441.
 [14] C. Santori, D. A. Fattal, J. Vuckovic, G. S. Solomon, Y. Yamamoto, *Nature* **2002**, 419, 594.
 [15] P. Maunz, D. L. Moehring, S. Olmschenk, K. C. Younge, D. N. Matsukevich, C. Monroe, *Nat. Phys.* **2007**, 3, 538.
 [16] A. Siphagil, M. L. Goldman, E. Togan, Y. Chu, M. Markham, D. J. Twitchen, A. S. Zibrov, A. Kubanek, M. D. Lukin, *Phys. Rev. Lett.* **2012**, 108, 143601.
 [17] A. Siphagil, K. D. Jahnke, L. J. Rogers, T. Teraji, J. Isoya, A. S. Zibrov, F. Jelezko, M. D. Lukin, *Phys. Rev. Lett.* **2014**, 113, 113602.
 [18] G. Di Martino, Y. Sonnefraud, M. S. Tame, S. Kéna-Cohen, F. Dieleman, i. m. c. K. Özdemir, M. S. Kim, S. A. Maier, *Phys. Rev. Applied* **2014**, 1, 034004.
 [19] T. B. Pittman, D. V. Strekalov, A. Migdall, M. H. Rubin, A. V. Sergienko, Y. H. Shih, *Phys. Rev. Lett.* **1996**, 77, 1917.
 [20] M. O. Scully, K. Drühl, *Phys. Rev. A* **1982**, 25, 2208.
 [21] R. Wiegner, C. Thiel, J. von Zanthier, G. S. Agarwal, *Opt. Lett.* **2011**, 36, 1512.
 [22] E. Megidish, A. Halevy, T. Shacham, T. Dvir, L. Dovrat, H. S. Eisenberg, *Phys. Rev. Lett.* **2013**, 110, 210403.
 [23] Z. Y. Ou, X. Y. Zou, L. J. Wang, L. Mandel, *Phys. Rev. A* **1990**, 42, 2957.
 [24] Y. H. Shih, A. V. Sergienko, M. H. Rubin, T. E. Kiess, C. O. Alley, *Phys. Rev. A* **1994**, 49, 4243.
 [25] J. G. Rarity, P. R. Tapster, E. Jakeman, T. Larchuk, R. A. Campos, M. C. Teich, B. E. A. Saleh, *Phys. Rev. Lett.* **1990**, 65, 1348.
 [26] V. Giovannetti, S. Lloyd, L. Maccone, *Science* **2004**, 306, 1330.
 [27] K. J. Resch, K. L. Pregnell, R. Prevedel, A. Gilchrist, G. J. Pryde, J. L. O'Brien, A. G. White, *Phys. Rev. Lett.* **2007**, 98, 223601.
 [28] T. Nagata, R. Okamoto, J. L. O'Brien, K. Sasaki, S. Takeuchi, *Science* **2007**, 316, 726.
 [29] J. Wen, S. Du, M. H. Rubin, *Phys. Rev. A* **2007**, 75, 033809.
 [30] V. Balić, D. A. Braje, P. Kolchin, G. Y. Yin, S. E. Harris, *Phys. Rev. Lett.* **2005**, 94, 183601.
 [31] P. Kolchin, S. Du, C. Belthangady, G. Y. Yin, S. E. Harris, *Phys. Rev. Lett.* **2006**, 97, 113602.
 [32] S. Zhang, C. Liu, S. Zhou, C. S. Chuu, M. M. T. Loy, S. Du, *Phys. Rev. Lett.* **2012**, 109, 263601.
 [33] D. Zhang, Y. Zhang, X. Li, D. Zhang, L. Cheng, C. Li, Y. Zhang, *Phys. Rev. A* **2017**, 96, 053849.
 [34] P. Chen, X. Guo, C. Shu, M. M. T. Loy, S. Du, *Optica* **2015**, 2, 505.
 [35] S. Zhang, J. F. Chen, C. Liu, M. M. T. Loy, G. K. L. Wong, S. Du, *Phys. Rev. Lett.* **2011**, 106, 243602.
 [36] T. M. Zhao, Y. S. Ihn, Y. H. Kim, *Phys. Rev. Lett.* **2019**, 122, 123607.
 [37] X. Guo, Y. Mei, S. Du, *Optica* **2017**, 4, 388.
 [38] S. Du, P. Kolchin, C. Belthangady, G. Y. Yin, S. E. Harris, *Phys. Rev. Lett.* **2008**, 100, 183603.

- [39] L. Zhao, X. Guo, C. Liu, Y. Sun, M. M. T. Loy, S. Du, *Optica* **2014**, *1*, 84.
- [40] P. Kolchin, *Phys. Rev. A* **2007**, *75*, 033814.
- [41] L. Zhao, Y. Su, S. Du, *Phys. Rev. A* **2016**, *93*, 033815.
- [42] J. Wen, S. Du, Y. Zhang, M. Xiao, M. H. Rubin, *Phys. Rev. A* **2008**, *77*, 033816.
- [43] C. H. R. Ooi, M. O. Scully, *Phys. Rev. A* **2007**, *76*, 043822.
- [44] J. Wen, S. Du, M. H. Rubin, *Phys. Rev. A* **2007**, *76*, 013825.
- [45] J. Wen, M. H. Rubin, *Phys. Rev. A* **2006**, *74*, 023809.
- [46] J. Wen, M. H. Rubin, *Phys. Rev. A* **2006**, *74*, 023808.
- [47] S. Du, J. Wen, M. H. Rubin, *Josa B* **2008**, *25*, C98.
- [48] H. Kim, M. L. Sang, S. M. Han, *Sci. Rep.* **2016**, *6*.